arXiv:1704.05669v1 [cond-mat.mtrl-sci] 19 Apr 2017

Electronic structure and charge density wave instability in $TiSe_2$: the effect of non-local exchange

Maria Hellgren,[1,2] Jacopo Baima,[1] Raffaello Bianco,[3,1] Matteo Calandra,[1] Francesco Mauri,[3,4] and Ludger Wirtz[2]

[1] *Institut de Minéralogie, de Physique des Matériaux et de Cosmochimie, Sorbonne Universités, Université Pierre et Marie Curie, CNRS, IRD, MNHN, 4 Place Jussieu, 75252 Paris, France*

[2] *Physics and Materials Science Research Unit, University of Luxembourg, 162a avenue de la Faïencerie, L-1511 Luxembourg, Luxembourg*

[3] *Dipartimento di Fisica, Universita di Roma La Sapienza, Piazzale Aldo Moro 5, I-00185 Roma, Italy*

[4] *Graphene Labs, Fondazione Istituto Italiano di Tecnologia, Via Morego, I-16163 Genova, Italy*

(Dated: April 20, 2017)

We show that the inclusion of screened exchange via hybrid functionals provides a unified description of the electronic and vibrational properties of $TiSe_2$. In contrast to local approximations in density functional theory, the explicit inclusion of exact, non-local exchange captures the effects of the electron-electron interaction needed to both separate the Ti-d states from the Se-p states and stabilize the charge-density-wave (CDW) (or low-T) phase via the formation of a $p-d$ hybridized state. We further show that this leads to an enhanced electron-phonon coupling that can drive the transition even if a small gap opens in the high-T phase. Finally, we demonstrate that a modified HSE functional generates a CDW phase where the electronic bands, the geometry, and the phonon frequencies are in agreement with experiments.

The charge density wave (CDW) instability is a common phenomenon in layered semi-metallic transition metal dichalcogenides (TMDs) [1] and has attracted considerable interest over the years, from both the experimental and the theoretical side. The CDW phase is sometimes found to compete with superconductivity and thus plays a similar role as the anti-ferromagnetic phase in strongly correlated heavy fermion systems or in high-T_c cuprates [2–5]. This intriguing similarity has stimulated the search for a better understanding of the physical mechanism behind the CDW instability in TMDs [6].

The CDW instability in $TiSe_2$ is one of the most studied and debated. On the experimental side, neutron diffraction [7] and X-ray scattering [8] have established the existence of a commensurate $2\times2\times2$ structural transition at 200 K. This is confirmed by angle resolved photo emission spectroscopy (ARPES) as well as by transport measurements, where an abrupt increase in resistivity is found at the same temperature. However, upon further cooling the resistivity reaches an anomalous maximum [7], after which a weak metallic behaviour is observed. By contrast, ARPES finds an insulating low-T phase, with a gap of approximately 0.1 eV [9–14]. In the high-T phase ARPES has not been able to conclude whether the system is semi-metallic or semi-conducting due to the very small indirect (possibly negative) gap. Theoretically, this fact makes $TiSe_2$ an ideal candidate to exhibit an excitonic insulator phase [9, 15–17] for which the CDW transition is driven by a purely electronic instability. Some recent experiments [18] partly support this scenario. On the other hand, excitonic correlations alone are insufficient as demonstrated in Ref. 19.

Additional experimental evidence for the CDW instability has been provided by vibrational spectra as a function of temperature. A complete softening of an optical phonon at the L-point has been observed in inelastic X-ray scattering experiments [20]. In Raman and infrared (IR) spectroscopy the transition is detected by the appearance of a large number of new modes [21, 22], some of which can be related to the CDW transition due to their strong temperature dependence.

On the theoretical side, first-principles calculations using density functional theory (DFT) within the local density approximation (LDA) or the semi-local PBE approximation correctly predict an imaginary phonon frequency at the CDW wave vector [20, 23, 24]. However, the large disagreement between the electronic band structure and ARPES measurements points to the need for improving the approximation to the exchange-correlation (XC) functional. It has been shown that the inclusion of non-local exchange gives a much better description of the electronic bands in both the high- and low-T phase [13, 14, 25, 26]. In Ref. 24 it was further shown that also the DFT+U approach improves the electronic band structure, bringing it into good agreement with ARPES spectra. This seeming improvement, however, was accompanied by a complete loss of the CDW instability.

In this work we provide a quantitative description of *both* the electronic band structure *and* the lattice dynamics of $TiSe_2$, and clarify the role of the electron-phonon interaction in driving the CDW transition. By an inclusion of screened exchange within hybrid functionals we capture the strong Coulomb repulsion due to the localised Ti-d-states, which is essential for an accurate description of the electronic band structure. In addition, we capture the long-range exchange interaction, which enhances the electron-phonon coupling that ultimately drives the CDW transition. To demonstrate that these ingredients

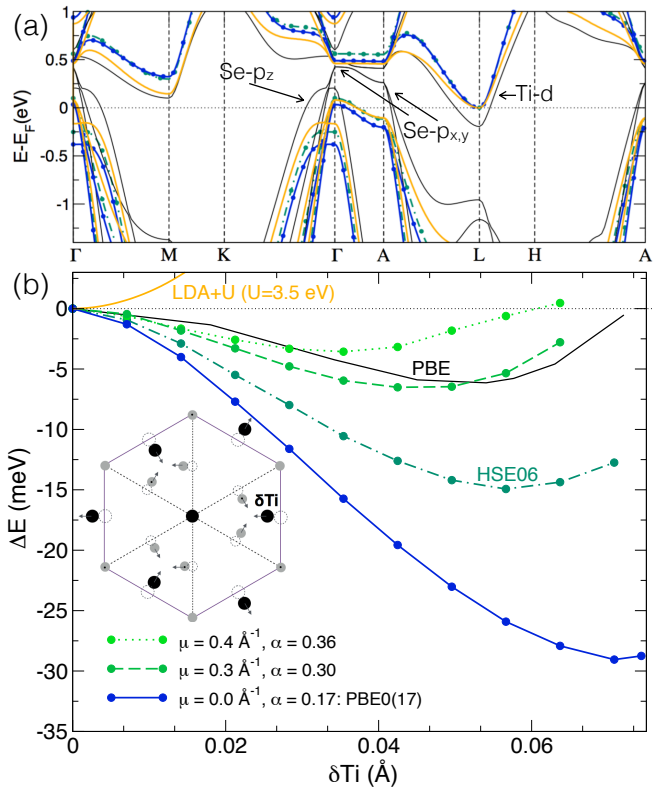

Figure 1. The upper panel (a) shows the band structure in the high-T phase in PBE (black solid line), HSE06 (green dash-dotted line and circles), PBE0(17) (blue solid line and circles) and LDA+U (U=3.5 eV) (orange solid line). The lower panel (b) shows the corresponding energy gain as a function of δTi. We show also the results obtained by varying the α and μ parameters such that the band structure around conduction band minimum and valence band maximum is the same as the one of HSE06 and LDA+U.

bring us close to a complete description of the XC effects in $TiSe_2$, we calculate the geometry, phonon frequencies, and the band structure of the high- and low-T phases with HSE06 [27] and a modified HSE functional, finding quantitative agreement with experiments.

$TiSe_2$ is a layered material which in the high-T phase (>200 K) crystallises in the space group $P\bar{3}m1$. The CDW phase is characterised by a 2×2×2 superstructure with a different space group $P\bar{3}c1$. The PBE phonon dispersion of the high-T phase was analysed in Refs. 23 and 24. The distortion pattern $\mathbf{d}_{3L}$ associated with the imaginary phonon frequncies at the three equivalent L points is of A_u symmetry and its projection on a single $TiSe_2$ layer is shown in the inset of Fig. 1(b). It is completely identified by its symmetry, the magnitude of the displacement δTi and the ratio δTi/δSe. The layers are held together by van der Waals forces and in the CDW phase adjacent layers are rotated by 60 degrees. In all calculations we use the experimentally determined a and c lattice parameters [28]. This choice indirectly accounts for van der Waals interaction due to the fixing of the interlayer distance [24]. Local functionals in DFT give rise to an excess of electron occupation on the Ti d-states compared to ARPES, mainly due to the large $p_z - d$ band overlap but also due to the overestimated $p_{x,y} - d$ band overlap (see black curve in Fig. 1 (a)). To cure this problem it is necessary to include the Coulomb repulsion or 'U' due to the localised Ti-d states. A simple corrective procedure to incorporate this effect is the DFT+U approach [29]. Indeed, in Ref. 24 it was shown that the $p-d$ band overlap reduced significantly (see orange curve Fig. 1 (a)). However, it was also found that the energy gain in the distortion quickly reduced by increasing 'U'.

Hybrid functionals incorporate 'U' [30], but in addition they capture the long-range exchange interaction. Although the hybrid functionals incorporate excitonic effects within time-dependent perturbation theory [31, 32] they only yield an approximate description of the multi-reference states required for a spontaneous formation of excitons as in the excitonic insulator model. The description of screening is quite simplified via a reduced pre-factor α and a range-separated Coulomb potential defined by μ. These parameters can be fitted in various ways but often the optimised HSE06 parameters ($\alpha = 0.25, \mu = 0.2\,\text{Å}^{-1}$) give good results [27]. In this work we have exploited the freedom of varying the parameters to shed light on the mechanism that drives the CDW transition in $TiSe_2$.

In Fig. 1 (a) we have summarised the results for the band structure in the high-T phase with different approximations [33] and different electronic structure codes [34–36]. In Fig. 1 (b) we plot the corresponding energy gain as a function of δTi by displacing the atoms according to the $\mathbf{d}_{3L}$ CDW pattern (using the experimentally determined ratio δTi/δSe = 3 [7]). We found HSE06 to give an enhanced negative curvature and energy gain of approximately a factor of 2 compared to PBE. This difference is mainly attributed to an overscreening at the PBE level due to the excess occupation on the Ti-d states, i.e., due to the overestimation of the metallicity of the system. However, this is not the complete picture. We see that the LDA+U and HSE06 approximations have almost identical band structures - both in rather good agreement with experiment [13, 14]. In LDA+U the instability is, however, absent. To explicitly demonstrate what is missing in LDA+U, we varied the parameters (α, μ) of the hybrid functionals such that the band gap is the same as in LDA+U (or HSE06). By reducing the range, i.e., by increasing μ, we could simulate LDA+U which acts only locally. As the range reduces the $p-d$ band overlap increases, so we simultaneously increased α in order to keep the band structure fixed. With $\mu = 0.3, 0.4\,\text{Å}^{-1}$ we found $\alpha = 0.3, 0.36$ respectively. It is clear that it is essential to keep the long-range potential in order to capture the instability.

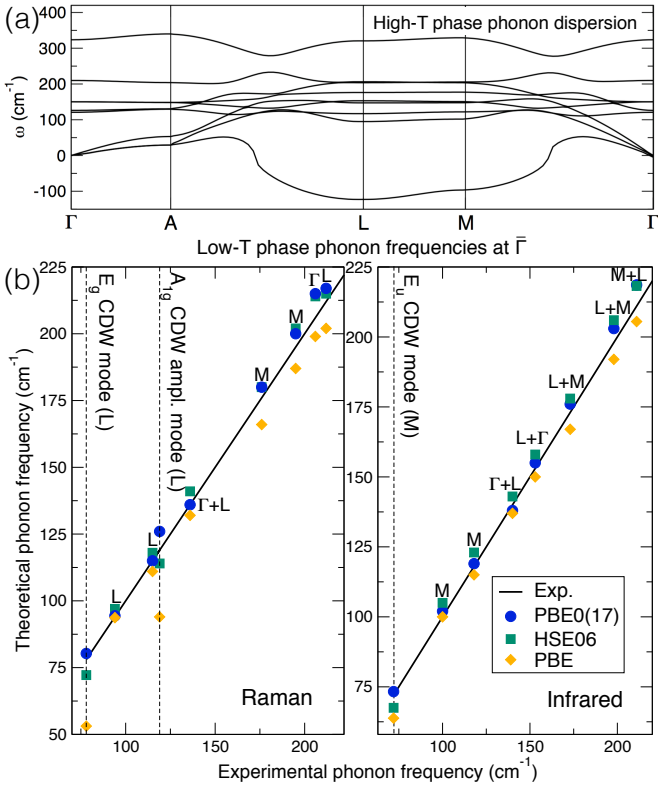

Figure 2. (a) Phonon dispersion of the high-T phase, calculated within HSE06. (b) Experimental[21, 37] versus calculated phonon frequencies of Raman and IR modes in the low-T phase. Modes related to the CDW distortion are marked by vertical dashed lines. The labels refer to the largest components of the back-folded phonon eigenvector with respect to the eigenvectors of the undistorted high T structure.

By increasing the range up to infinity (again keeping the gap fixed to HSE06), we generate an approximation similar to PBE0 but with $\alpha = 0.17$. We will refer to this approximation as PBE0(17). With this functional, the energy gain increases substantially as does the amplitude of the distortion. After relaxing the atomic positions in the CDW phase, we find $\delta\mathrm{Ti} = 0.055, 0.061, 0.082$ Å with PBE, HSE06 and PBE0(17) respectively. In experiment, $\delta\mathrm{Ti} = 0.085 \pm 0.014$ Å [7], which thus supports the approximation with infinite range. Based on the above analysis we will continue to discuss the mechanism for the CDW transition, but first we study the CDW phase as obtained within HSE06 and PBE0(17).

The electronic band structure in comparison with ARPES suggests that the CDW phase is accurately captured with hybrid functionals [14]. However, as seen above, a good description of the band structure alone is not sufficient to judge the quality of the XC approximation. The vibrational frequencies are proportional to the second derivative of the energy and thus provide an additional stringent test for the validity of different approximations. We have calculated the harmonic Raman and IR active phonon frequencies in the CDW phase within HSE06 and PBE0(17) using a finite difference approach as implemented in the `CRYSTAL` code [38].

In Fig. 2 we compare the theoretical frequencies with low-T experimental Raman [37] and IR [21] frequencies (at 11 K and 20 K, respectively). We analyze the spectra of the CDW phase by back-folding of the phonons at A, L and M of the high-T phase Brillouin zone (see HSE06 phonon dispersion [39] in Fig. 2 (a)) onto the $\bar{\Gamma}$ point of the low-T phase Brillouin zone. For all three functionals, we find an overall good agreement with the experimental results. However, there are three notable exceptions of particular interest for this work: these are the modes related to the instabilities of the high-T structure (marked by vertical dashed lines). The three-fold degenerate imaginary phonon frequency at L splits into one A_{1g} and a two-fold degenerate E_g mode, which are both Raman active. These have been previously identified as being related to the CDW transition from their experimental temperature dependence [21, 22]. The A_{1g} (amplitude) mode corresponds to the oscillations of the CDW order parameter. The imaginary phonon frequency at M similarly gives rise to an E_u IR active phonon, corresponding to the peak found at around 75 cm^{-1} in experimental spectra, and to one A_{1u} inactive mode. The frequencies of these modes are systematically underestimated by PBE (20% and 30% for the A_{1g} and E_g modes, respectively). Already HSE06 brings these frequencies in much better agreement with experiment (now underestimated by 4% and 7%, respectively). PBE0(17), which gave the best geometry and overall phonon frequencies, also gives the best CDW mode frequencies (overestimated by 5% and 2%, respectively). Since the frequencies of these modes depend very sensitively on the CDW potential energy surface (compare Fig. 1 (b)), the reproduction of these modes by the hybrid functionals is an important confirmation that they reliably reproduce the electronic structure of $TiSe_2$.

With a reliable description of the vibrational and electronic properties, we can now analyze in detail the physical mechanism that is responsible for the CDW instability in $TiSe_2$. Fig. 3 (a) shows the HSE06 band structure in both the low-T and high-T phase (the latter one is back-folded into the Brillouin zone that corresponds to the 2×2×2 supercell of the low-T phase). The high-symmetry points of the 2×2×2 supercell are marked with a bar. At the CDW distortion, the three-fold degenerate Ti-d band splits into a band with dominant d_{z^2} character derived from the Ti atom in the supercell that does not move with the distortion, and a two-fold degenerate band with Ti-d and Se-p hybridization around $\bar{\Gamma}$ due to the interaction between the p and d states. Similarly, the two-fold degenerate Se-p bands move to lower energy and hybridize with Ti-d states around $\bar{\Gamma}$. Such $p-d$ hybridization, discussed also in Refs. 11 and 40, is observed by studying the site-projected orbitals onto spher-

ical harmonics before and after the transition. Panel (b) presents a zoom of the region around $\bar{\Gamma}$, showing the effect of a small $\mathbf{d}_{3L}$ distortion on the electronic structure. We see that the distortion only changes the $p-d$ gap while leaving the rest of the electronic structure unaffected. We can therefore assume that it is mainly the $p-d$ states around $\bar{\Gamma}$ which are involved in the transition and extract the EPC, or, more precisely, the deformation potential $\mathcal{D}$ for the different functionals. The deformation potential is defined as $\mathcal{D} = \langle \bar{\Gamma}d|\delta V/\delta d_{3L}|\bar{\Gamma}p\rangle$, where the variation of the total self-consistent potential V is taken with respect to the magnitude d_{3L} of the $\mathbf{d}_{3L}$ distortion of A_u symmetry and periodicity L (see Eq. 9 in Ref. 24). The states $|\bar{\Gamma}d\rangle$ and $|\bar{\Gamma}p\rangle$ with energy difference $\mathcal{E}_0$ are obtained from the Ti-d and Se-p states at L and Γ in the undistorted unit cell by back-folding them onto $\bar{\Gamma}$ in the supercell. Without loss of generality, all quantities can be taken as real in the supercell. The p and d states are superimposed and illustrated in Fig. 3 (c) together with the $p-d$ hybridized state in the CDW phase. We also note from first order perturbation theory that $\mathcal{D} = \langle \delta(\bar{\Gamma}d)/\delta d_{3L}|\bar{\Gamma}p\rangle \times \mathcal{E}_0$ and hence (at fixed $\mathcal{E}_0$) $\mathcal{D}$ measures the overlap between the variation of the d state with the distortion and the undistorted p state. We then obtain $\mathcal{D}$ using a finite difference approach [41]. At small but finite d_{3L} we construct the 2×2 submatrix of the Hamiltonian $\mathcal{H}$: $\mathcal{H}_{dd} = -\mathcal{E}_0/2+\mathcal{O}(d_{3L}^2)$, $\mathcal{H}_{pp} = \mathcal{E}_0/2+\mathcal{O}(d_{3L}^2)$ and $\mathcal{H}_{pd} = \mathcal{H}_{dp} = \mathcal{D}d_{3L}+\mathcal{O}(d_{3L}^2)$ and diagonalize it to obtain $\mathcal{D}^2 = \frac{1}{4}(\mathcal{E}^2-\mathcal{E}_0^2)/d_{3L}^2$, where $\mathcal{E}$ is the $p-d$ gap upon the distortion and we have discarded the higher order terms in d_{3L}. The results obtained from this procedure can be found in Fig. 3 (d). Although some coupling already exists between p and d states at the PBE level, the deformation potential (and so the EPC) is strongly enhanced via the inclusion of non-local (or long-range) exchange. The PBE0(17) functional enhances $\mathcal{D}^2$ by a factor of 5 and HSE06 by a factor of 2.5. The same trend is seen in Figs. 1 (b) and 3 (d) and we can conclude that whereas all functionals (except PBE) give similar band structures in the undistorted phase, the $p-d$ gap after a small distortion critically depends on the range of exchange, resulting in a higher deformation potential. Our result goes in line with some previous findings that the EPC can be strongly enhanced by non-local exchange, notably in weakly doped 2D materials [41–44] and some high-T_c superconductors [45]. We notice, however, that in $TiSe_2$ the exchange interaction has two competing effects: it increases the band gap of the high-T phase which suppresses the instability, but it also increases the deformation potential which enhances the instability. The first effect is mostly due to short-range exchange and the second due to long-range effects. Although the band structure in HSE06, which we used as a reference, has a small negative $p-d$ gap (-0.1 eV) in the high-T phase, the instability does not crucially depend on the existence of a Fermi surface. In fact, due

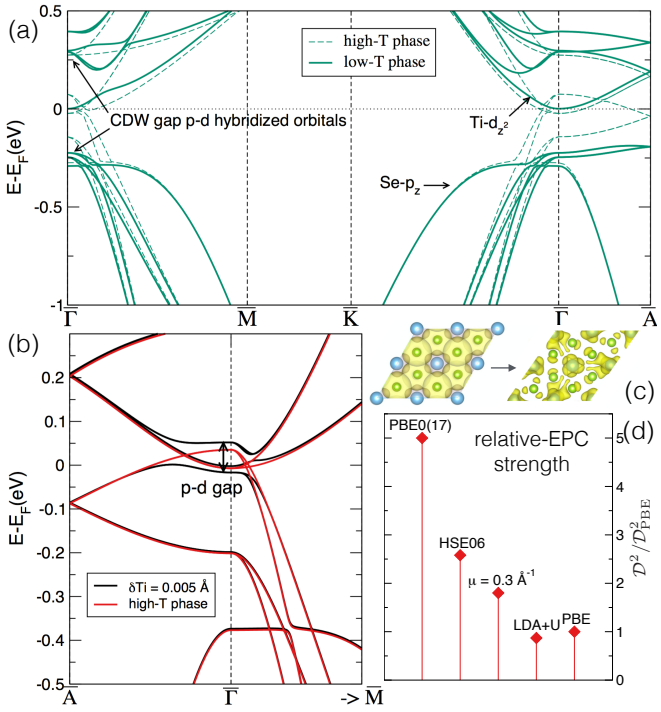

Figure 3. (a) HSE06 band-structure of undistorted (high-T) and CDW (low-T) phases of $TiSe_2$. Panel (b) shows a zoom around the Fermi level demonstrating the mixing of the Ti-d with the Se-$p_{x,y}$ levels (as denoted in Fig. 1). The EPC between these states is calculated for various functionals (panel (d)). The value for $\mathcal{D}^2_{\rm PBE} = 8\,\mathrm{eV}^2/\mathrm{Å}^2$ (calculated with respect to δTi displacement). Panel (c) demonstrates the mixing (hybridization) of these orbitals [46] in the CDW phase.

to the enhanced EPC, the CDW phase can exist even if the gap in the high-T phase is positive, as observed in, e.g., a mono-layer $TiSe_2$ [13]. This is easily demonstrated by increasing the amount of exact exchange (α). With $\mu = 0.2\,\mathrm{Å}^{-1}$ fixed, the instability persists up to $\alpha = 0.35$ when the gap is as large as 0.2 eV. At larger values of the gap (or α) the hybridization of Ti-d -and Se-$p_{x,y}$ bands is suppressed and the instability disappears.

In conclusion, our work solves the long standing problem of the simultaneous description of the electronic band structure and vibrational properties of $TiSe_2$. Previous *ab-initio* studies of the energetics of $TiSe_2$ were performed at the level of DFT with local functionals. In that case, the direct band gap is strongly underestimated resulting in large Se-p and Ti-d band overlaps in the high-T phase. Using exact, non-local exchange disentangles the bands and renders the electron-phonon coupling mechanism in the CDW distortion visible.

M.H. and L.W. gratefully acknowledge financial support from the FNR (projects RPA-phonon and INTER/ANR/13/20/NANOTMD). The authors acknowledge support from the European Union Horizon 2020 research and innovation programme under Grant agree-

ment No. 696656-GrapheneCore1. and by Agence Nationale de la Recherche under the reference n. ANR-13-IS10-0003-01 and by Prace. Calculations were performed at IDRIS, CINES, CEA and BSC TGCC. The authors are grateful to K. Rossnagel, for having supplied to them the image data of ARPES experiment.

[1] J. A. Wilson, F. J. D. Salvo, and S. Mahajan, Advances in Physics **24**, 117 (1975).
[2] S. Y. Li, G. Wu, X. H. Chen, and L. Taillefer, Phys. Rev. Lett. **99**, 107001 (2007).
[3] A. F. Kusmartseva, B. Sipos, H. Berger, L. Forró, and E. Tutiš, Phys. Rev. Lett. **103**, 236401 (2009).
[4] E. Morosan, H. W. Zandbergen, B. S. Dennis, J. W. G. Bos, Y. Onose, T. Klimczuk, A. P. Ramirez, N. P. Ong, and R. J. Cava, Nat Phys **2**, 544 (2006).
[5] D. Qian, D. Hsieh, L. Wray, E. Morosan, N. L. Wang, Y. Xia, R. J. Cava, and M. Z. Hasan, Phys. Rev. Lett. **98**, 117007 (2007).
[6] K. Rossnagel, J. Phys.: Condens. Matter **23**, 213001 (2011).
[7] F. J. Di Salvo, D. E. Moncton, and J. V. Waszczak, Phys. Rev. B **14**, 4321 (1976).
[8] Y. I. Joe, X. M. Chen, P. Ghaemi, K. D. Finkelstein, G. A. de la Pena, Y. Gan, J. C. T. Lee, S. Yuan, J. Geck, G. J. MacDougall, T. C. Chiang, S. L. Cooper, E. Fradkin, and P. Abbamonte, Nat Phys **10**, 421 (2014).
[9] T. Pillo, J. Hayoz, H. Berger, F. Lévy, L. Schlapbach, and P. Aebi, Phys. Rev. B **61**, 16213 (2000).
[10] T. E. Kidd, T. Miller, M. Y. Chou, and T.-C. Chiang, Phys. Rev. Lett. **88**, 226402 (2002).
[11] K. Rossnagel, L. Kipp, and M. Skibowski, Phys. Rev. B **65**, 235101 (2002).
[12] H. Cercellier, C. Monney, F. Clerc, C. Battaglia, L. Despont, M. G. Garnier, H. Beck, P. Aebi, L. Patthey, H. Berger, and L. Forró, Phys. Rev. Lett. **99**, 146403 (2007).
[13] P. Chen, Y. H. Chan, X. Y. Fang, Y. Zhang, M. Y. Chou, S. K. Mo, Z. Hussain, A. V. Fedorov, and T. C. Chiang, Nature Commun. **6**, 8943 (2015).
[14] Y.-H. P. Chen, X. Chan, S. Fang, Z. Mo, Z. Hussain, A. V. Fedorov, M. Chou, and T. C. Chiang, Scientific Reports **6**, 37910 (2016).
[15] D. Jérome, T. M. Rice, and W. Kohn, Phys. Rev. **158**, 462 (1967).
[16] C. Monney, H. Cercellier, F. Clerc, C. Battaglia, E. F. Schwier, C. Didiot, M. G. Garnier, H. Beck, P. Aebi, H. Berger, L. Forró, and L. Patthey, Phys. Rev. B **79**, 045116 (2009).
[17] C. Monney, C. Battaglia, H. Cercellier, P. Aebi, and H. Beck, Phys. Rev. Lett. **106**, 106404 (2011).
[18] T. Rohwer, S. Hellmann, M. Wiesenmayer, C. Sohrt, A. Stange, B. Slomski, A. Carr, Y. Liu, L. M. Avila, M. Kallane, S. Mathias, L. Kipp, K. Rossnagel, and M. Bauer, Nature **471**, 490 (2011).
[19] M. Porer, U. Leierseder, J. M. Ménard, H. Dachraoui, L. Mouchliadis, I. E. Perakis, U. Heinzmann, J. Demsar, K. Rossnagel, and R. Huber, Nat Mater **13**, 857 (2014).
[20] F. Weber, S. Rosenkranz, J.-P. Castellan, R. Osborn, G. Karapetrov, R. Hott, R. Heid, K.-P. Bohnen, and A. Alatas, Phys. Rev. Lett. **107**, 266401 (2011).
[21] J. A. Holy, K. C. Woo, M. V. Klein, and F. C. Brown, Phys. Rev. B **16**, 3628 (1977).
[22] C. S. Snow, J. F. Karpus, S. L. Cooper, T. E. Kidd, and T.-C. Chiang, Phys. Rev. Lett. **91**, 136402 (2003).
[23] M. Calandra and F. Mauri, Phys. Rev. Lett. **106**, 196406 (2011).
[24] R. Bianco, M. Calandra, and F. Mauri, Phys. Rev. B **92**, 094107 (2015).
[25] Z. Zhu, Y. Cheng, and U. Schwingenschlögl, Phys. Rev. B **85**, 245133 (2012).
[26] M. Cazzaniga, H. Cercellier, M. Holzmann, C. Monney, P. Aebi, G. Onida, and V. Olevano, Phys. Rev. B **85**, 195111 (2012).
[27] J. Heyd, G. E. Scuseria, and M. Ernzerhof, The Journal of Chemical Physics **118**, 8207 (2003).
[28] Due to the neglect of dispersion forces experimental lattice constants ($a = 3.54\,\text{Å}, c = 6.008\,\text{Å}$) were used throughout this work.
[29] V. I. Anisimov, J. Zaanen, and O. K. Andersen, Phys. Rev. B **44**, 943 (1991).
[30] B. Himmetoglu, A. Floris, S. de Gironcoli, and M. Cococcioni, International Journal of Quantum Chemistry **114**, 14 (2014).
[31] J. Paier, M. Marsman, and G. Kresse, Phys. Rev. B **78**, 121201 (2008).
[32] A.-M. Ferrari, R. Orlando, and M. Rerat, J. Chem. Theory and Comput. **11**, 3245 (2015).
[33] Calculations with PBE and LDA+U have been obtained with Quantum ESPRESSO [34] and calculations with HSE06 have been obtained with VASP [35, 47] within the projector-augmented-wave (PAW) method [48]. A plane-wave cut-off of 320 eV was used and semi-core electrons were included in the Ti PAW potential. Results were converged with a $24\times24\times12$ k-point mesh in the high-T cell. For most calculations presented in this manuscript we used the all-electron `CRYSTAL` code [36] with an adapted molecular def2-TZVP basis set for solid state calculations. The results for the energy gain in HSE06 was within 1 meV/supercell in agreement between VASP and `CRYSTAL`.
[34] P. Giannozzi *et al*, J. Phys.: Condens. Matter **21**, 395502 (2009).
[35] G. Kresse and J. Furthmüller, Comput. Mater. Sci. **6**, 15 (1996).
[36] R. Dovesi, R. Orlando, A. Erba, C. M. Zicovich-Wilson, B. Civalleri, S. Casassa, L. Maschio, M. Ferrabone, M. D. L. Pierre, P. Darco, Y. Noel, M. Causa, M. Rerat, and B. Kirtman, Int. J. Quantum Chem. **114**, 1287 (2014).
[37] S. Sugai, K. Murase, S. Uchida, and S. Tanaka, Solid State Communications **35**, 433 (1980).
[38] F. Pascale, C. Zicovich-Wilson, F. Lopez, B. Civalleri, R. Orlando, and R. Dovesi, J. Comput. Chem. **25**, 888 (2004).
[39] The phonon dispersion is approximated on a 2×2×2 q-grid.
[40] N. G. Stoffel, S. D. Kevan, and N. V. Smith, Phys. Rev. B **31**, 8049 (1985).
[41] M. Lazzeri, C. Attaccalite, L. Wirtz, and F. Mauri, Phys. Rev. B **78**, 081406 (2008).
[42] C. Attaccalite, L. Wirtz, M. Lazzeri, F. Mauri, and A. Rubio, Nano Letters **10**, 1172 (2010).
[43] M. Calandra, P. Zoccante, and F. Mauri, Phys. Rev.

Lett. **114**, 077001 (2015).
[44] B. Pamuk, J. Baima, R. Dovesi, M. Calandra, and F. Mauri, Phys. Rev. B **94**, 035101 (2016).
[45] Z. P. Yin, A. Kutepov, and G. Kotliar, Phys. Rev. X **3**, 021011 (2013).
[46] The iso-surface of the square of the Bloch orbitals were obtained within HSE06 using VASP and VESTA (K. Momma and F. Izumi, J. Appl. Crystallogr., 44, 1272 (2011)).
[47] G. Kresse and J. Furthmüller, Phys. Rev. B **54**, 11169 (1996).
[48] G. Kresse and D. Joubert, Phys. Rev. B **59**, 1758 (1999).